Title	H+ implanted channel waveguides in buried epitaxial crystalline YAG:Nd, Tm layers and infrared-to-blue upconversion characterization
Authors	Szachowicz, Marta;Joubert, Marie-France;Moretti, Paul;Couchaud, Maurice;Ferrand, Bemard;Borca, Camelia;Boudrioua, Azzedine
Publication date	2008-12-01
Original Citation	Szachowicz, M., Joubert, M.-F., Moretti, P., Couchaud, M., Ferrand, B., Borca, C. and Boudrioua, A. (2008) 'H+ implanted channel waveguides in buried epitaxial crystalline YAG:Nd,Tm layers and infrared-to-blue upconversion characterization', Journal of Applied Physics, 104(11), pp. 113104. doi: 10.1063/1.2976303
Type of publication	Article (peer-reviewed)
Link to publisher's version	http://aip.scitation.org/doi/abs/10.1063/1.2976303 - 10.1063/1.2976303
Rights	© 2008 American Institute of Physics, This article may be downloaded for personal use only. Any other use requires prior permission of the author and AIP Publishing. The following article appeared in Szachowicz, M., Joubert, M.-F., Moretti, P., Couchaud, M., Ferrand, B., Borca, C. and Boudrioua, A. (2008) 'H+ implanted channel waveguides in buried epitaxial crystalline YAG:Nd,Tm layers and infrared-to-blue upconversion characterization', Journal of Applied Physics, 104(11), pp. 113104. doi: 10.1063/1.2976303 and may be found at http://aip.scitation.org/doi/abs/10.1063/1.2976303
Download date	2023-05-05 08:42:39
Item downloaded from	http://hdl.handle.net/10468/4219

University College Cork, Ireland
Coláiste na hOllscoile Corcaigh

H^+ implanted channel waveguides in buried epitaxial crystalline YAG:Nd,Tm layers and infrared-to-blue upconversion characterization

Marta Szachowicz, Marie-France Joubert, Paul Moretti, Maurice Couchaud, Bemard Ferrand, Camelia Borca, and Azzedine Boudrioua

Citation: Journal of Applied Physics **104**, 113104 (2008); doi: 10.1063/1.2976303
View online: http://dx.doi.org/10.1063/1.2976303
View Table of Contents: http://aip.scitation.org/toc/jap/104/11
Published by the American Institute of Physics

H^+ implanted channel waveguides in buried epitaxial crystalline YAG:Nd,Tm layers and infrared-to-blue upconversion characterization

Marta Szachowicz,[1,a)] Marie-France Joubert,[1] Paul Moretti,[1,b)] Maurice Couchaud,[2] Bemard Ferrand,[2] Camelia Borca,[3,c)] and Azzedine Boudrioua[4]
[1]*Laboratoire de Physico-Chimie des Matériaux Luminescents, Université de Lyon, F-69622, Lyon, France; Université Lyon 1, Villeurbanne; CNRS, UMR 5620, Laboratoire de Physico-Chimie des Matériaux Luminescents*
[2]*LETI/DOPT/CEA-Grenoble, 17 Rue des Martyrs, 38054 Grenoble Cedex 9, France*
[3]*EPFL/STI/IOA/APL, BM 4.124, Station 17, Lausanne CH-1015, Switzerland*
[4]*Laboratoire Matériaux Optiques, Photoniques et Systèmes (MOPS), CLOES, CNRS-FRE-2304, Université de Metz et Supélec, 2 Rue E. Belin, 57078 Technopole 2000 Metz Cedex 3, France*

(Received 7 May 2008; accepted 7 July 2008; published online 1 December 2008)

Nd,Tm:YAG codoped single crystal waveguides were studied in order to discover if the presence of Nd^{3+} ions favors blue luminescence at 486 nm. Innovative implantation techniques were applied to locally change Δn and form varied H^+ implanted channel structures in Nd,Tm:YAG buried epitaxial waveguiding layers. The guided blue luminescence due to the Tm^{3+} $^1G_4 \rightarrow {}^3H_6$ transition was studied under infrared excitation at 785 nm (Tm^{3+} absorption) and 808 nm (Nd^{3+} absorption) for the epitaxial planar waveguides of different Tm^{3+} and Nd^{3+} concentrations for all the implanted channel waveguide structures. © *2008 American Institute of Physics*. [DOI: 10.1063/1.2976303]

I. INTRODUCTION

Solid state, compact, blue emitting laser devices of micrometric dimensions are topical issues for optical data processing. This stimulates research on optical microwaveguides, planar, and of limited width in rare-earth ion-doped crystalline materials. In fact, on the one hand, some of the rare-earth ions embedded in dielectric crystals are characterized by an intense emission in the blue spectral range, either after one-step direct excitation or after infrared upconversion excitation. On the other hand, the waveguiding structures associate with the high effective absorption and emission cross sections of the active ion in the crystal lattice with the effects of confinement and guiding in order to obtain laser action.

The amplification of Nd^{3+} emission at 1.064 μm in Nd:YAG (yttrium aluminum garnet) epitaxial waveguides has been widely studied. A recent work revealed that the presence of a trace amount of Tm^{3+} in such amplifiers produces a blue emission arising out of the absorption of photons at 1.064 μm in the Tm^{3+} $^3H_4$ excited level.[1] Since this blue emission coming from the Tm^{3+} $^1G_4 \rightarrow {}^3H_6$ transition previously gave rise to the laser effect at 486 nm under excited state absorption (ESA) pumping with two photons of 785 and 638 nm in the Tm:YAG bulk crystal,[2] we decided to study single crystal Nd,Tm:YAG waveguides in order to elucidate if the Nd^{3+} ions were likely to favor 486 nm blue laser action under pumping with only one laser beam. No infrared to blue upconversion emission from $^1G_4$ manifold has been observed to date in Tm:YAG with single wavelength excitation. Interaction between thulium and ytterbium ions[3,4] or between thulium and holmium ions[5] was investigated and gave rise to upconverted blue fluorescence under single wavelength excitation around 930–970 nm (Yb^{3+} $^2F_{7/2} \rightarrow 2F_{5/2}$ transition) or 785 nm (Tm^{3+} $^3H_6 \rightarrow {}^3H_4$ transition), respectively, but lasing under such configuration has never been reported.

The route toward effective formation of waveguiding structures still presents a challenge. It concerns notably two-dimensional waveguide manufacturing in rare-earth ion-doped crystalline materials both in bulk and layer forms. Ion implantation is the only method that up to now has been effectively applied to about 100 various materials.[6–8] The high versatility of the physical preparation process is due to the fact that its parameters are easily controllable. Moreover the intrinsic properties of light ion (He^+,H^+) implanted materials seem to be preserved to a remarkable extent. The examples described in Ref. 8 are a good illustration. In particular, continuous-wave laser operation was reported in Nd:YAG (Refs. 9–11) and in Ti:sapphire[12] implanted waveguides, while upconversion was demonstrated in Er:YAG.[13]

We have developed a route for index structuring a crystal surface, i.e., to fabricate channel waveguides, by using a specific slit-based setup and multiple implantation sequences.[14] This technique has been applied recently to Er:$YAlO_3$ (YAP) bulk crystals[15] and Nd,Tm:YAG epitaxial layers[16] resulting in proton implanted channel waveguide formation. Infrared to green and infrared to blue upconversion luminescence, respectively, were demonstrated in the created structures. Following these results we present here a detailed study of various Nd,Tm:YAG layers covered with epitaxial undoped YAG. Their thorough understanding as a source of blue light could provide a means for developing miniature upconversion lasers for integrated optics. This paper devel-

[a)]Present address: Tyndall National Institute, University College Cork, Lee Maltings, Prospect Row, Cork, Ireland.
[b)]Electronic mail: pmoretti@pcml.univ-lyonl.fr.
[c)]Present address: Swiss Light Source and the Laboratory for Waste Management, Paul Scherrer Institute, Viligen PSI CH-5232, Switzerland.

ops ideas described previously[16] and will focus both on channel waveguide fabrication issues, especially regarding the implantation parameters, which were varied in a large range, and on a detailed spectroscopic study of the Nd,Tm codoped YAG material. The latter will concern the luminescence from the epitaxial planar waveguides as well as the channel structures implanted within them. Hence the Tm^{3+} and Nd^{3+} concentrations will be of principal significance; however the way of implantation will contribute as well to the spectroscopic analysis.

This paper consists of five sections. We will start from the explanation of the methods used in the Nd,Tm:YAG channel waveguide fabrication and the physical mechanisms governing them. After a short description of the experimental methods, the detailed characterization of the obtained waveguides will be presented, as well as the results of their spectroscopic study. Finally, the results will be summarized.

II. WAVEGUIDE PREPARATION AND CONDITIONING

Two kinds of waveguides are studied: epitaxial active layers of Nd,Tm:YAG with positive index change enhanced in relation to undoped YAG by the presence of bismuth oxide in the epitaxial bath and channel waveguides formed by the H^+ implantation method in these active layers.

A. Epitaxial planar waveguide realization and conditioning

Active layers of Nd,Tm,Bi:YAG were grown in LETI/DOPT/CEA-Grenoble by a liquid-phase epitaxy (LPE) process on YAG substrates and subsequently covered by epitaxial undoped YAG. Consequently, buried planar waveguides were obtained. LPE consists of crystal growth by setting the substrate in contact with a liquid source. The precipitation of an element in the supersaturated liquid solution (including in our case Nd^{3+}, Tm^{3+} and bismuth oxide) results in the formation of a crystalline layer of the same, or very closely related, crystalline lattice nature as that of the substrate. The samples were then cut and carefully polished in order to obtain end faces of very high optical quality. Two different Nd^{3+} and various Tm^{3+} concentrations were used in the following configurations: for Nd^{3+} at 2.5%, Tm^{3+} concentration was 0.05% or 0.1% and for Nd^{3+} at 1%, four concentrations of Tm^{3+} were set at 0.1%, 1%, 2%, or 3%. The samples had two different dimensions, 4×6 or 4×4 mm^2, and therefore had two propagation lengths. The cover thickness was between 9.2 and 10 μm (nevertheless, every layer had its "uncover" counterpart), while the active layer thickness varied between 2.6 and 4.5 μm. Such preformed buried planar waveguides were then implanted in order to form channel structures.

B. Implanted channel waveguide preparation

The planar waveguide formation by the ion implantation process is based on its simplest form on the homogenous irradiation of a bulk crystal surface. The incident ions, when they travel through material, lose their energy in two ways: by inelastic electronic collisions and by elastic nuclear collisions. As far as light ions are concerned (i.e., H^+ or He^+), the electronic losses (by ionization and excitation processes) dominate (98%) in slowing down the ions. Yet the stopping region, where the crystal lattice becomes damaged and, as a result, its density is generally lowered, is determined by the nuclear collisions. In most materials, an optical barrier is observed in the ion nuclear stopping region because of an induced negative index change. The layer buried several microns beneath the surface allows therefore light confinement and guiding between itself and the surface. Nevertheless, for a narrow group of materials, such as YAG (Ref. 17) or LIF,[18] some small positive index change caused by the electronic energy deposition is observed. It can be sufficient to confine low order modes. A nontunneling well type index profile is obtained in that case. Even more unusual, an index increase has been also reported in the damaged area itself.[17,19] The origin of such positive index variation is still in debate. Recently a model has been proposed to explain the specific behavior of both types of refractive index changes in He^+-implanted $LiNbO_3$ waveguides.[20] Note furthermore that heavier ions (B^{3+},Si^+,C^+,P^+) have also been used to fabricate waveguides in crystals with either negative or positive reported index variations.[21–24] In any case, a vertical light confinement was obtained.

Channel waveguide formation requires the implantation process to be modified in order to ensure additionally the lateral light confinement. Different techniques were proposed to limit the implanted area[9,25,26] generally by using photolithographically patterned masks. In contrast with lithography based masking techniques, we use a direct one stage method. As described in Ref. 14, a moving slit of controlled width is placed above the sample and serves as a mask window allowing implanting striped areas. Moreover, with our setup, the implantations can be performed in well-controlled sequences in order to form several narrow layers at various depths that create all together one vertical implanted region. These layers are implanted at a fixed energy while the incident angle of the beam is adjusted for each of them to obtain a stopping region at a given depth. Originally such a manner of index structuring consisted of many successive weak similar dose implantations, which formed together an almost continuously implanted area. In later works this principle was slightly modified so that the dose was varied with the incident beam angle in order to compensate the longitudinal straggling of the ions—thereby obtaining a more or less flat damage profile in all the implanted layers.[15]

In fact, the channel formation depends on the crystal nature and implantation parameters. As already discussed, either negative ($\Delta n<0$) or positive ($\Delta n>0$) index change may be induced by the energy deposition process. The implanted areas act therefore, respectively, either as vertical barriers to laterally confine the light between them or are themselves the channels. In the former case, when a bulk crystal is implanted, an additional planar implantation is necessary to limit the channel by a bottom barrier. However, because our epitaxial active layers are themselves planar waveguides, such limitation is here unnecessary.

Once waveguides are formed in a material, propagation losses have to be minimized. Among the sources of losses in waveguides, light scattering at the waveguide surface is one

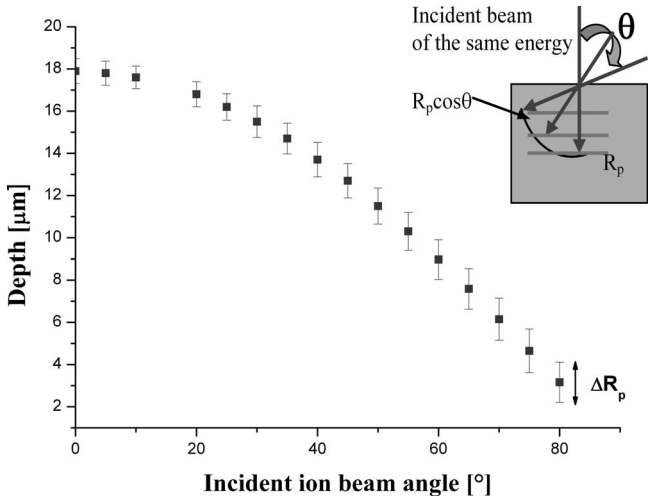

FIG. 1. The H^+ implantation depths in YAG calculated by the SRIM program for a fixed energy of 1.5 MeV and various incident ion beam angles. ΔRp is the mean projected range of the ions. The inset illustrates the principle of implantation for a constant but with a variation in the angle of the incident beam—several vertical stopping regions are obtained.

of the most important. Burying deeply the waveguide beneath the surface is the most efficient way to suppress this process, and that is the main reason why we decided to use covered doped planar layers. Moreover, another dominant loss source peculiar to implanted waveguides originates from absorption due to color centers created during implantation. These are related to trapped charges at isolated point defects. To eliminate this problem postimplant thermal annealing is frequently applied.

Since our aim was to obtain deep implants through the thick YAG cover, we decided to use H^+ ions instead of He^+. The energy of incident protons remained fixed at 1.5 MeV for all implantations. The objective was to locally modify the index of the active Tm,Nd codoped layer, of thickness between 2.6 and 4.5 μm, which was deeply buried at 9.2–10 μm beneath the surface. The irradiation angles were therefore chosen "on average" according to the results of SRIM calculations[27] reported in Fig. 1.

We applied a variety of implantation parameters, including very innovative ones, in order to generate various index changes. Starting from many successive weak-dose implantations (first results in YAG have been demonstrated recently[14]), we applied strong dose implantations in the sequences of three or seven angles. Finally we tried a very simple one-angle implantation. In Fig. 2 all the investigated implanted structures are presented together.

1. Implantation A

Assuming that low-dose implantation leads to a positive index change in the YAG material (as demonstrated in Ref. 14), three channel waveguides of different widths were initially produced [hereafter described as implantation A—see Fig. 2(a)] by sequences of seven implantations with angles in the 20°–50° range and weak doses between 2×10^{15} and 3×10^{15} ions/cm^2 for each angle (total dose 2×10^{16} ions/cm^2).

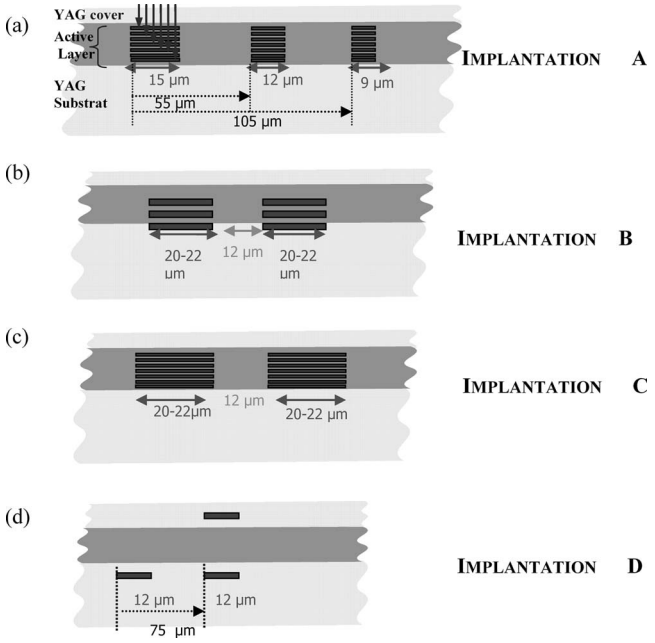

FIG. 2. Structures formed by H^+ implantation with (a) seven-angle sequence with weak dose, (b) three-angle sequence with strong or very strong doses, (c) seven-angle sequence with strong dose, and (d) simple single implantations.

2. Implantations B and C

The purpose of the implantation shown in Figs. 2(b) and 2(c) was fundamentally different. We expected to damage an implanted region to such degree that a negative change in refraction index would be induced. Two lateral barriers (width of 20–22 μm) of negative index change were therefore to be created with the result that one channel between them (10–12 μm) was supposed to be obtained. Two kinds of implantation were performed to try to achieve this goal. Three-angle sequences [named B, see Fig. 2(b)] at 25°, 35°, and 45° with strong doses of 2×10^{16}, 3×10^{16}, and 2×10^{16} ions/cm^2, respectively, or even stronger ones of 5×10^{16} ions/cm^2 were applied for each angle. The implantation named C [see Fig. 2(c)] consisted of seven-angle sequences in the 20°–50° range with a relatively strong dose of 0.9×10^{16} ions/cm^2 for each angle value.

3. Implantation D

Finally, we performed single implantations at high dose (3×10^{16} ions/cm^2), either slightly below or from both sides of the active layer [named D, see Fig. 2(d)]. The latter aimed to achieve a better localization of light in the active layer. The incident angle values were adjusted according to the SRIM simulation in Fig. 1 to assure the right position of the damaged regions relative to the active layer.

III. EXPERIMENTAL SETUP FOR GUIDING AND SPECTROSCOPIC CHARACTERIZATION

The waveguiding and spectroscopic properties were investigated by end-fire coupling. An optical fiber or a ×20 microscope objective was used to launch the light into the waveguide, while a ×20 (or ×50) microscope objective collected the output light. Either a continuous wave argon ion

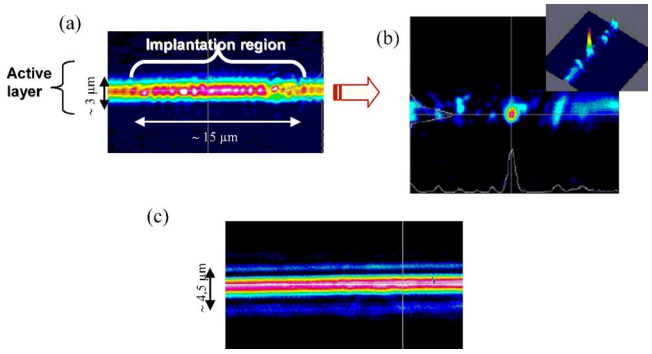

FIG. 3. (Color online) (a) and (b) Output images of a 15 μm width channel waveguide formed in the A-implantation conditions (see Fig. 2). The laser excitation wavelength is 785 nm, the structure is strongly multimode (a) but by adjusting the injection conditions the fundamental mode can be excited (b). (c) Output image of the active planar epitaxial layer excited at 632 nm.

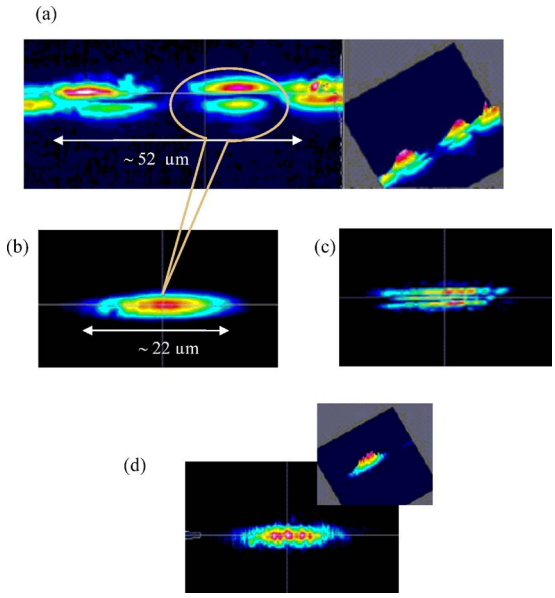

FIG. 4. (Color online) Mode patterns of three-angle channel waveguides implanted at strong dose (implantation B). (a) Two waveguides excited simultaneously at 785 nm and corresponding to two adjacent implanted regions. One waveguide under an excitation of (b) 785 nm, (c) 488 nm, and (d) 785 nm, but filtered with a CORION LS 550 –F-T783 filter selecting the blue upconverted guided emission.

laser (488 nm), He–Ne laser (632 nm), or sapphire titanium laser (710–840 nm wavelength range) was used as launching laser sources. The confined light intensity in the planar or channel waveguides was analyzed with a charge coupled device (CCD) camera placed above the sample to investigate propagating losses. The losses were also measured in the active planar layer by a method based on a dark line spectroscopy setup, as presented in Ref. 28. The outcoupled guided intensities for two in-coupling positions of the prism were measured and compared, while the in-coupling conditions were carefully controlled. This method was applied to specific samples without YAG covers; hence, epitaxial planar layers were not buried in this case.

For spectroscopic analysis of the Tm^{3+} blue fluorescence and the Nd^{3+} IR luminescence, the same end-fire setup was used, but the output light was filtered by a monochromator and detected with a photomultiplier or a germanium cell, respectively. In addition, for time analysis, the titanium-sapphire laser beam was modulated by means of a chopper.

IV. WAVEGUIDE CHARACTERIZATION

As expected, implantation A resulted in three waveguides related to the three implanted areas with enhanced index change. The structures were multimode [Fig. 3(a)]. However, under optimized injection conditions, it was possible to excite the zero order mode, as shown in Fig. 3(b) for 785 nm excitation. In Fig. 3(c) the CCD camera output image of the epitaxial planar waveguide shows that the layer is multimode, hence, one should pay attention that the channel dimension is actually more extensive in the vertical direction than it seems to be in Fig. 3(a).

The effect of the three-angle strong implantation B was much more surprising. Two channel waveguides, with positive index change, corresponding to the two implanted areas were observed instead of one between them. Figure 4(a) shows simultaneous injection in the two implanted areas. Figure 4(b) demonstrates one of these waveguides displayed under infrared excitation at 785 nm. Since the structure is quite large, the injection in the waveguides is relatively simple. Both of the waveguides are well defined for the high dose $[(2-3)\times 10^{16}$ ions/cm$^2]$ as well as for the very high dose $(5\times 10^{16}$ ions/cm$^2)$ implantation. Furthermore it was possible to excite different modes of the structure, particularly in the vertical direction. As seen in Fig. 4(c), as compared to Fig. 4(a), thinner and more closely spaced modes are observed when a shorter excitation wavelength is used (488 nm). Vertically, the waveguiding structure seems therefore to sustain two and three modes at 785 and 488 nm, respectively, while horizontally it remains highly multimode. Finally, Fig. 4(d) depicts the filtered output image of a waveguide excited at 785 nm, thus selecting the blue upconverted guided emission only, which is the object of the detailed spectroscopic investigations described in the next section.

Another attempt to form a one channel waveguide between two implanted areas was performed with a more uniform distribution of implanted regions with respect to the active layer. Thus the implantation C in Fig. 2(c) brought together the conditions presented above: on the one hand, relatively strong doses were retained and on the other, the number of implantation angles was increased up to seven. The total dose was hence very similar to the strong dose implantation B $(6.3\times 10^{16}$ and 7×10^{16} ions/cm^2, respectively), but the implanted ions were, in this case, more continuously distributed in the whole depth of the epitaxial layer. Although the output image seems to be different, the behavior of the refractive index was in principle the same as for three-angle implantation B. Positive index changes were observed directly in the two striped implanted zones (32 μm one to the other). Yet the lateral confinement of the modes was better in comparison to implantation B, as seen in Fig. 5(a). This indicates that a stronger index variation has been induced. Essentially, the two implanted structures appeared coupled and the modes observed were generally distributed not only in the implanted areas but also between them [see Fig. 5(b)]. In fact, the three regions, i.e., two implantation

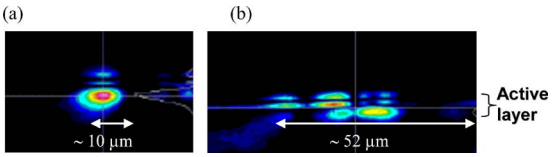

FIG. 5. (Color online) Outcoupled intensity distribution (excitation at 785 nm) of seven-angle channel waveguides implanted at strong dose: (a) fundamental mode excited in one implanted area and (b) coupling effect between two nearby implanted areas.

areas and the transition between them, should be better perceived as one complex structure. Indeed, it has to be remembered that the epitaxial layer is actually a planar waveguide itself. In reality, this behavior could also be attributed to the former implantation B. It is less clearly observed very likely because the index enhancement induced in the implanted areas was lower. Furthermore, these two "complex structures," B and C, can be described as multimodal ones horizontally as well as vertically [Figs. 4(a) and 5(b)]. To achieve two well-separated and uncoupled waveguides, the distance between the implanted areas should be increased significantly.

Once the irradiation effect on the refractive index performance was discovered, i.e., a positive Δn directly in the irradiated zone, the simple strong dose implantations (D) were also tested. One simple strong dose implantation turned out to be sufficient to obtain a channel waveguide, as shown on the output CCD images given in Fig. 6. For the two-angle implanted structure, i.e., with two damaged layers above and below the active layer [see Fig. 2(d)], the output light was less intense and more elliptical; however the difference was rather small. In this case, a very weak light confinement was also observed nearby the surface. A twice-higher total dose could very likely induce a very weak index change enhancement also in the cover.

After annealing of the B implanted samples in air at 350 °C for 3 h, we observed that the shape of the modes in the waveguides became even more regular and their vertical position was strictly limited to the epitaxial layer level. However, a systematic study of the annealing effect on the implanted waveguide properties was not carried out. Nevertheless, it is worth noting that good light confinement was already obtained in all as-implanted samples.

The light propagation was also analyzed under excitation at 488 nm (wavelength in the Tm^{3+} blue emission range) by means of a CCD camera placed above the sample. The observed light diffusion was very small, but a qualitative difference between the channel and the planar waveguide, in

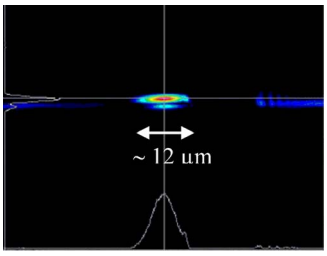

FIG. 6. (Color online) Zero order mode of 785 nm laser light outcoupled at the epitaxial layer level of a simple single-implanted channel waveguide [Implantation conditions, see Fig. 2(d)].

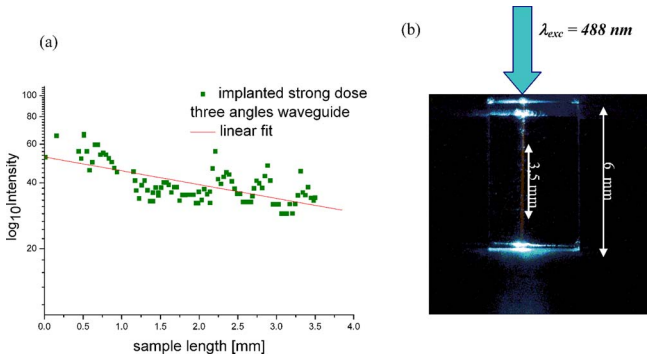

FIG. 7. (Color online) Estimation of the losses in a three-angle waveguide implanted at strong dose. (a) The confined light intensity analyzed as a function of propagation distance and (b) the top view of the propagating light in the sample excited at 488 nm.

favor of the former, could be clearly perceived. To estimate the order of this difference in losses, the intensity of the guided light was measured as a function of the propagation distance for both epitaxial planar waveguide and a channel one. An example of such measurements (for implantation B) is shown in Fig. 7 along with the related CCD image. Using the known formula for the attenuation coefficient $\boldsymbol{\alpha}_{\mathrm{dB/cm}} = -(\mathbf{1}/\boldsymbol{l})\mathbf{10}\log(\boldsymbol{I}_{\mathrm{final}}/\boldsymbol{I}_{\mathrm{initial}})$, where l is the propagation distance, the planar/channel waveguide loss ratio was evaluated to be around 3. One has to be aware however that such calculations are only estimates, especially as the waveguides are buried beneath the surface. The losses in epitaxial planar waveguides without a cover were then measured by the specific m-line based setup.[28] They were estimated to be of the order of 1 dB/cm. According to the ratio value, we can therefore conclude that the losses in the channel are very likely less than 0.5 dB/cm.

To summarize, although our investigations on proton implantation effects in the YAG epitaxial layers were conducted over a quite large dose range, surprisingly it was impossible to create negative index variation to form channels between two vertical side optical barriers. If it is argued, as commonly claimed, that positive and negative index changes are related to electronic energy deposition and damage collisions process, respectively [as this is for instance very well illustrated in LIF (Ref. 18)], we have to conclude that the former is largely the dominant effect in proton implanted YAG. To reverse such a situation, two ways could be tested: (1) implantation with doses higher than 10^{17} ions/cm^2, nevertheless at the cost of a higher number of color centers and higher stress that would be produced; very likely they would degrade strongly the waveguiding and spectroscopic properties and (2) implanting at low temperature in order to allow sufficient permanent damage formation if some self-annealing effects occur. On the other hand, a further hypothesis on the origin of index variations could be put forward: both energy deposition processes produce positive index change. Anomalous index increases in the damage area have been actually demonstrated in very few cases. In $LiNbO_3$ it was observed in one of the indices (extraordinary);[19,20] however, implantation was performed with He^+ ions and in a specific very low dose range ($2-4\times10^{15}$ ions/cm^2). In YAG (Ref. 14) this index behavior occurred, while multiple

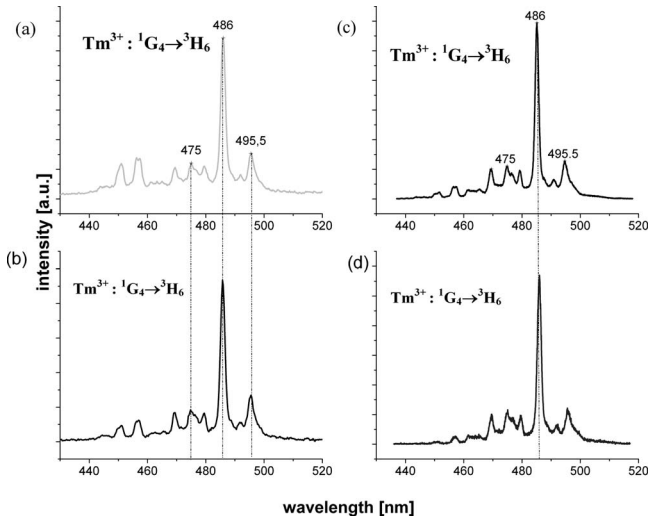

FIG. 8. Comparison of the blue Tm emission spectra under IR excitation in the bulk, a planar active layer, and a weak-dose implanted waveguide. (a) YAG:Tm 5% bulk crystal, $\lambda_{exc}=785$ nm (Tm^{3+}). (b) Lateral light emission of a YAG:Bi,Tm 0.1%, Nd 2.5% planar waveguide excited at $\lambda_{exc}=808$ nm (Nd^{3+}). (c) Endcoupled guided light from a YAG:Bi,Tm 1%, Nd 1% planar waveguide excited at $\lambda_{exc}=785$ nm (Tm^{3+}). (d) Outcoupled light emission of a YAG:Bi,Tm 1%, Nd 1% channel waveguide under $\lambda_{exc}=785$ nm (Tm^{3+}).

He^+ implantations at low dose (0.75×10^{16} ions/cm^2) were used. As a matter of fact, positive index variation is highly valuable because the modes are completely confined in the optical well with no tunneling losses. It is further to be noted that quite efficient light propagation was obtained in all our as-implanted samples. This means that proton, in contrast to helium[14] implantation, does not create too many absorbing color centers in YAG.

V. BLUE EMISSION SPECTROSCOPIC STUDY

The emission spectra in the blue spectral range were collected under excitation at 785 nm (Tm^{3+} absorption) or 808 nm (Nd^{3+} absorption) for the six epitaxial planar waveguides of different Tm^{3+} and Nd^{3+} concentrations, as well as for all the implanted channel waveguides. Moreover they were compared with the luminescence spectra from singly doped Tm:YAG excited at 785 nm. In Fig. 8, such comparison is presented between a 5% Tm:YAG bulk crystal emission, the lateral emission from the 2.5% Nd, 0.1% Tm:YAG epitaxial planar waveguide, the guided emission from the 1% Nd, 1% Tm:YAG epitaxial planar waveguide, and the guided emission from a channel waveguide implanted in this last layer. The most intense emission band is centered at 486 nm and belongs to the Tm^{3+} ${}^1G_4 \rightarrow {}^3H_6$ transition, which spans from 460 to 500 nm. The shape of this emission spectrum depends neither on the rare-earth ion concentration, the excitation wavelength, the kind of structure (bulk, planar, or channel waveguide), nor the implantation procedure and remains the same for all the cases considered. The weak structure appearing for wavelengths below 460 nm is attributed to the Tm^{3+} ${}^1D_2 \rightarrow {}^3H_5$ transition. Its intensity relative to the ${}^1G_4 \rightarrow {}^3H_6$ structure differs from one spectrum to another due to differences in excitation powers. This is not surprising because a larger number of pump photons are involved in populating the ${}^1D_2$ than in populating the ${}^1G_4$ level.[16] Moreover, for excitation at 808 nm, several emission peaks around 550 nm corresponding to the Nd^{3+} ${}^4G_{7/2} \rightarrow {}^4I_{9/2}$ transition were observed, possibly due to IR to green upconversion within the Nd^{3+} ions. The most striking difference between Tm^{3+} singly doped bulk crystal/epitaxial layers and Tm^{3+},Nd^{3+} codoped waveguides was found in the intensity level of emitted blue fluorescence. Under 785 nm excitation and fixed excitation power conditions, the blue emission in the bulk 5% Tm:YAG was very weak; in Tm:YAG epitaxial layers (Tm concentrations between 1.5% and 3.5%) it was almost undetectable, while in the codoped waveguides it was extremely bright. Furthermore, the intensity increases with the Tm^{3+} concentration to 2% Tm, then the intensity decreases by more than 50% for the 3% Tm,Nd:YAG waveguide. However since its width is smaller in comparison with the others, it may be a result of poorer light injection into the waveguide. Additionally the blue upconverted luminescence intensifies with the ion dose used for the fabrication of implanted channel waveguides. A detailed quantitative measure was rather difficult in this case because of the complicated nature of the structures and, what follows, unrepeatable conditions for light injection into a waveguide. However the implanted channel giving the most intense output signal was the strong dose three-angle implanted structure presented in Figs. 2(b) and 4(b).

Excitation spectra for the 486 nm upconverted light were compared with the absorption spectra of the singly doped bulk crystals 0.9% Nd:YAG and 0.5% Tm:YAG. Figure 9 presents such comparison for the case of the 2.5% Nd, 0.1% Tm:YAG planar waveguide, where the collected emission was either the guided blue luminescence at the output of the waveguide [Fig. 9(b)] or the blue emission breaking waveguide laterally [Fig. 9(c)]. In the later case, the absorption lines of both of the active ions were detected in the excitation spectrum of Tm,Nd codoped YAG. In case of the guided blue luminescence, only Tm^{3+} absorption lines were observed in the spectrum. This phenomenon can be attributed to the saturation of Nd^{3+} ion absorption along the waveguide. Moreover all excitation spectra of the 1064 nm Nd^{3+} emission were saturated, especially for the guided IR light, or when collected laterally at the end of the sample. Indeed the Nd^{3+} concentration at 2.5% is rather high. That is why the Nd^{3+} concentration was decreased to 1% in the samples designed for the implantation process, and the excitation spectra of such planar epitaxial waveguides demonstrated Tm^{3+} absorption lines as well as Nd^{3+} lines [Fig. 9(d)] for each of the four Tm^{3+} concentrations (0.1%, 1%, 2%, and 3%). The saturation effect of Nd^{3+} ion absorption along 1% Nd doped waveguides was not observed. Nevertheless it turned out that the way of the implantation also influences excitation spectra. In Fig. 10 the excitation spectra of channel waveguides fabricated under different conditions are compared. For the stronger dose several angle implantations, Nd^{3+} absorption lines were not discernible in the spectrum. However for the weak-dose implanted waveguides or even more for the very simple implanted structures, both kinds of lines were distinguishable. It can be suggested that the nuclear collision processes during the implantation are responsible for changes in

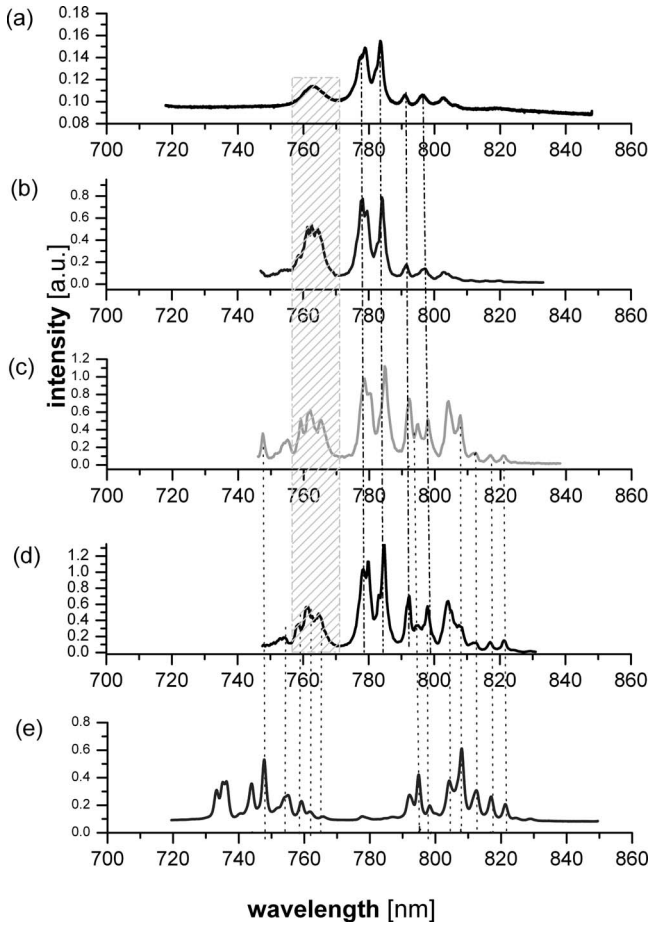

FIG. 9. Absorption spectra in doped bulk crystals and excitation spectra of the visible emission (486 nm) in various planar layers. (a) YAG: 0.5% Tm^{3+} bulk crystal absorption spectrum. Excitation spectra in a Bi 2.5%, Nd 0.1% Tm:YAG layer. (b) Light endcoupled. (c) Laterally collected light. (d) Light endcoupled in a Bi 1%, Nd 2% Tm:YAG layer. (e) YAG:Nd^{3+} 0.9% bulk crystal absorption spectrum.

the Nd-Tm interactions in the material. Indeed never before have channel waveguides been implanted in codoped YAG, hence it is difficult to draw a comparison with Nd doped YAG, where such an effect did not take place.[14] What is interesting is that after 3 h annealing at 350 °C of a strongly implanted sample (implantation B), the Nd^{3+} lines in the excitation spectrum of the guided blue luminescence became discernible, although weakly. This may support the hypothesis of ion rearrangements in the H^+ stopping region, where the crystal lattice becomes damaged leading to perturbation of the Nd-Tm interactions.

The blue luminescence dynamics study showed that with the 1% Nd, 2% Tm:YAG waveguide, whatever is the excitation wavelength, the steady state rise time of the upconverted blue fluorescence was about 4 ms. Under 808 nm excitation (Nd^{3+} absorption), decreasing Tm^{3+} concentration leads to a gradual slowing down of this rise time, whereas there is no detectable change under 785 nm excitation (Tm^{3+} absorption). In Fig. 11 a plot of the blue fluorescence intensity versus the excitation power shows a slope of 1.6 in logarithmic scale.

The energy level structures of Tm^{3+} in Tm:YAG (Ref. 29) and of Nd^{3+} in Nd:YAG (Ref. 30) are well known, and a scheme is presented in Fig. 12. It appears from our results that the presence of neodymium ions is essential for efficient blue emission of thulium ions under IR excitation. The question is: what is the process responsible for this efficient IR to blue upconversion in Nd,Tm codoped YAG? The well known emission spectrum due to Nd^{3+} $^4F_{3/2} \rightarrow {}^4I_{11/2}$ transition in YAG was recorded in all the epitaxial planar and implanted channel Nd,Tm:YAG waveguides under excitation at 785 nm (Tm^{3+} absorption) or 808 nm (Nd^{3+} absorption). It was also recorded under 808 nm excitation with the singly doped Nd:YAG waveguides. The shape of this emission spectrum was identical regardless of the presence or absence of Tm^{3+} in the waveguide and whatever is the excitation wavelength. This constitutes evidence that the process responsible for the blue emission from Tm^{3+} ions is not $^3H_4$ ESA of photons emitted by Nd^{3+} ions at 1.064 μm or at any other wavelength of the $^4F_{3/2} \rightarrow {}^4I_{11/2}$ transition. The process responsible for the intense blue fluorescence, emitted following excitation either in resonance with one of the Nd^{3+} $^4I_{9/2} \rightarrow {}^4F_{5/2} + {}^2H(2)_{9/2}$ absorption lines or in resonance with one of the Tm^{3+} $^3H_6 \rightarrow {}^3H_4$ absorption lines, is the energy transfer upconversion described below. Excitation at 808 nm leads to population of the Nd^{3+} $^4F_{5/2} + {}^2H(2)_{9/2}$ level as well as to population of the Tm^{3+} $^3H_4$ state due to direct Nd^{3+} $^4F_{5/2} + {}^2H(2)_{9/2}$ absorption on the one hand and energy transfer on the other hand $(Nd^{3+}[{}^4F_{5/2} + {}^2H(2)_{9/2}] + Tm^{3+}({}^3H_6) \rightarrow Nd^{3+}({}^4I_{9/2}) + Tm^{3+}({}^3H_4)$; point dotted arrows in Fig. 12). Similarly, excitation at 785 nm leads to population of Tm^{3+} $^3H_4$ state as well as to population of the Nd^{3+} $^4F_{5/2} + {}^2H(2)_{9/2}$ level due to direct Tm^{3+} $^3H_4$ absorption and energy transfer $(Tm^{3+}({}^3H_4) + Nd^{3+}({}^4I_{9/2}) \rightarrow Tm^{3+}({}^3H_6) + Nd^{3+}[{}^4F_{5/2}\,{}^2H(2)_{9/2}]$; square dotted arrows in Fig. 12). The Tm^{3+} blue emission is then favored due to the nonradiative transfer

$$Nd^{3+}({}^4F_{3/2}) + Tm^{3+}({}^3H_4) \rightarrow Nd^{3+}({}^4I_{11/2}) + Tm^{3+}({}^1G_4),$$

a process that brought out as well for tellurite glass.[31]

VI. CONCLUSION

We have demonstrated the feasibility of producing channel waveguides in crystalline layers of YAG:Tm,Nd epitaxially deposited on YAG crystals. They were deeply buried under an epitaxially grown YAG cover. We index structured these active planar layers by means of H^+-ion single or multiple implantations. The implantation depths were adjusted by controlling the beam angle with the irradiated surface. Several structures were fabricated by varying the implantation parameters and their propagating properties were investigated. The dose, local and total, was in particular wide ranging. Surprisingly, we observed only positive index changes in all implanted structures, allowing therefore direct writing of channels even for doses as high as 5×10^{16} ions/cm^2. Index variation by electronic energy deposition was very likely the dominant process. However, a contribution to the positive index variation from collision-damaging processes cannot be completely ruled out, especially if the damage is not retained in the aftermath of self-annealing effects during implantation. The channel

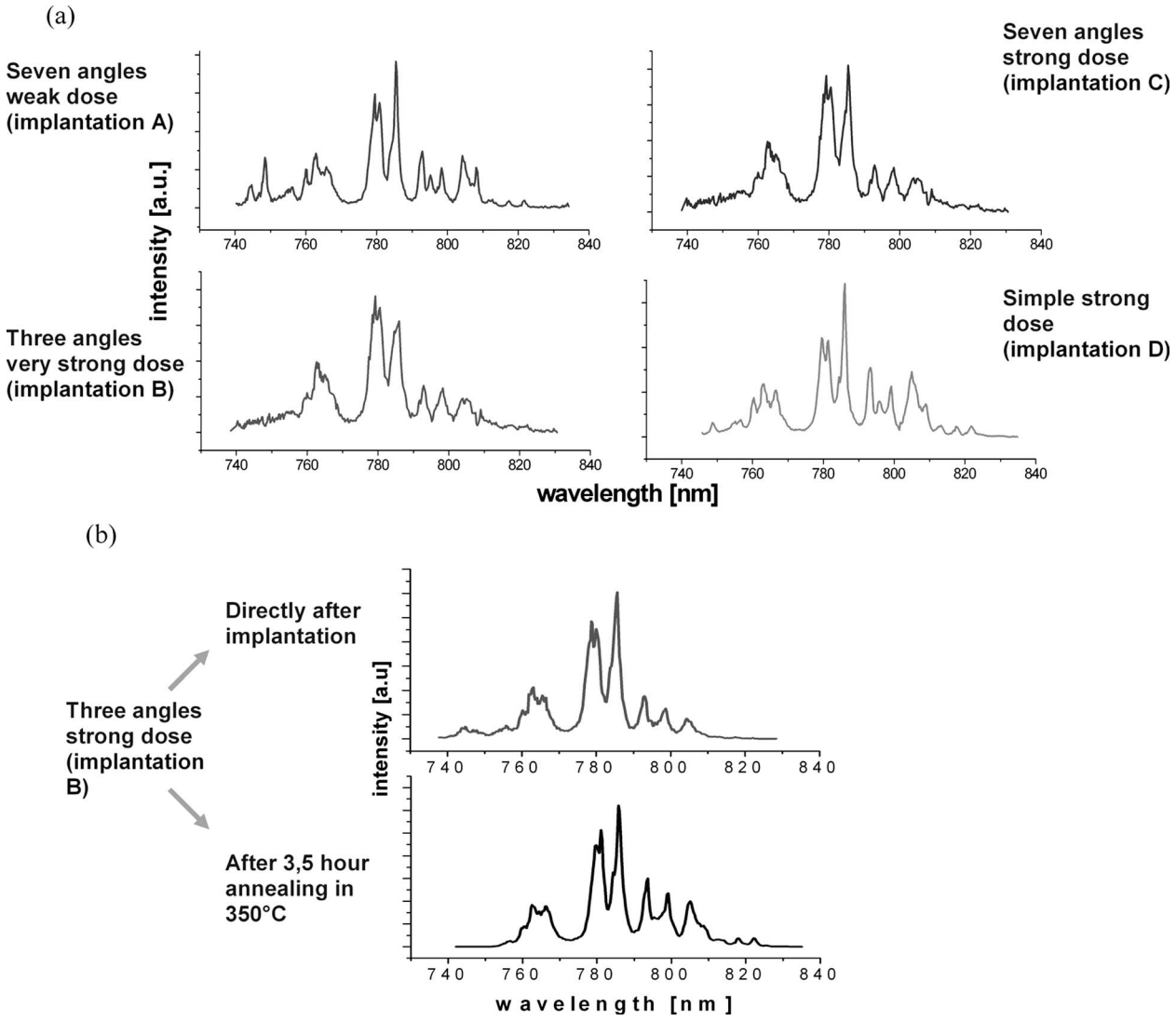

FIG. 10. Excitation spectra (emission wavelength: 486 nm) recorded at the output of a Bi 1%, Nd 2% Tm:YAG channel waveguides. (a) Effects of the implantation conditions. (b) Annealing effect in a three-angle waveguide implanted at a strong dose.

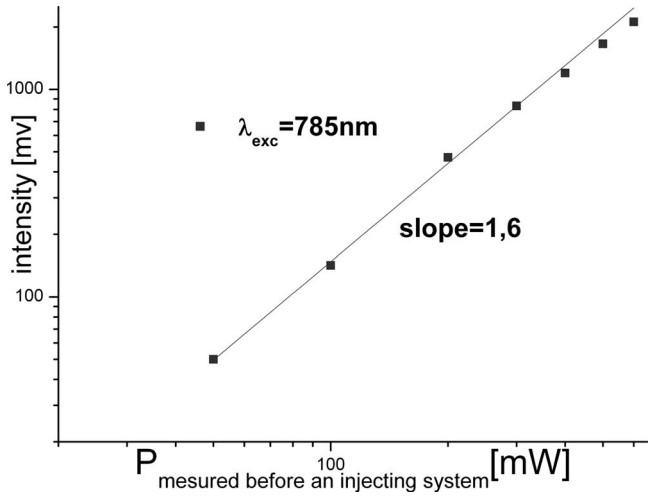

FIG. 11. Example of blue fluorescence intensity (logarithmic scale) recorded at the output of a channel waveguide as a function of the IR excitation power.

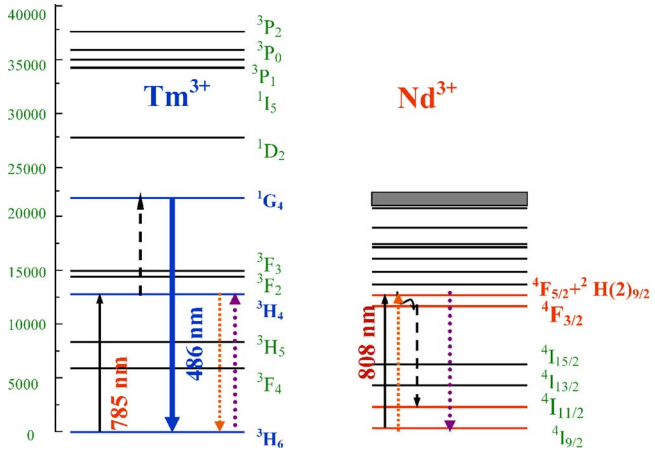

FIG. 12. (Color online) Energy level scheme of Tm^{3+} and Nd^{3+} in YAG and energy transfer upconversion mechanism responsible for the blue emission in the codoped crystal.

structure giving the most intense blue fluorescence output signal was obtained by a triple high-dose implant. However, it is worth noting that all the as-implanted structures could be excited and give rise to upconversion blue emission. The measured losses were estimated to be below 1 dB/cm. Post-annealing treatment was applied only for preliminary testing. Undoubtedly a systematic and detailed study of annealing effects combined with an optimization of the implantation parameters should improve significantly the propagating properties, allowing in particular the fabrication of a single mode waveguide.

Moreover, the emission spectra of the implanted structures were investigated in the blue spectral range under excitation at 785 nm (Tm^{3+} absorption) or 808 nm (Nd^{3+} absorption) with various Tm^{3+} and Nd^{3+} concentrations. Intense Tm^{3+} emission peaked at 486 nm was observed with steady state rise time of about 4 ms. Its shape and position are independent of the nature of the waveguide structure and the rare-earth concentration, and its intensity increases with the Tm^{3+} concentration at least to 2% of Tm^{3+}. An important result of our investigation is that the Nd^{3+} codoping does favor considerably the Tm^{3+} blue emission due to an efficient energy transfer upconversion process.

In conclusion, further optimization of the channel structure should allow generating blue upconverted laser emission.

[1]L. Brassé, Ph.D. thesis, Université Joseph Fourier, 2000.
[2]B. P. Scott, F. Zhao, R. S. F. Chang, and N. Djeu, Opt. Lett. **18**, 113 (1993).
[3]A. Knüpfer, V. Ostroumov, E. Heumann, G. Huber, and V. Lupei, J. Phys. (Paris), Colloq. **4**, C4-501 (1994).
[4]P. J. Morris, W. L¸thy, H. P. Weber, Y. D. Zavartsev, P. A. Studenikin, A. F. Umiskov, and A. I. Zagumenyi, CLEO/EUROPE'94, Presentation CFB1 (unpublished).
[5]M. Falconieri, A. Lanzi, G. Salvetti, and A. Toncelli, Opt. Mater. **7**, 135 (1997).
[6]P. D. Townsend, P. J. Chandler, and L. Zhang, *Optical Effects of Ion Implantation* (Cambridge University Press, Cambridge, 1994).
[7]P. D. Townsend, Nucl. Instrum. Methods Phys. Res. B **89**, 270 (1994).
[8]F. Chen, X.-L. Wang, and K.-M. Wang, Opt. Mater. **29**, 1543 (2007).
[9]S. J. Field, D. C. Hanna, A. C. Large, D. P. Shepherd, A. C. Tropper, P. J. Chandler, P. D. Townsend, and L. Zhang, Electron. Lett. **27**, 2375 (1991).
[10]E. Flores-Romeo, G. V. Vázquez, H. Marquez, R. Range-Rojo, J. Richards, and R. Trejo-Luna, Opt. Express **12**, 2264 (2004).
[11]M. Domenech, G. V. Vázquez, E. Cantelar, and G. Lifante, Appl. Phys. Lett. **83**, 4110 (2003).
[12]C. Grivas, D. P. Shepherd, R.W. Eason, L. Laversenne, P. Moretti, C. Borca, and M. Pollnau, Opt. Lett. **31**, 3450 (2006).
[13]X. Huang, N. Cutinha, A. Alcazar de Velasco, P. J. Chandler, and P. D. Townsend, Nucl. Instrum. Methods Phys. Res. B **142**, 50 (1998).
[14]P. Moretti, M.-F. Joubert, S. Tascu, B. Jacquier, M. Kaczkan, M. Malinowskii, and J. Samecki, Opt. Mater. **24**, 315 (2003).
[15]M. Szachowicz, S. Tascu, M.-F. Joubert, P. Moretti, and M. Nikl, Opt. Mater. **28**, 162 (2006).
[16]M. Szachowicz, P. Moretti, M.-F. Joubert, M. Couchaud, and B. Ferrand, Appl. Phys. Lett. **90**, 031113 (2007).
[17]L. Zhang, P. J. Chandler, P. D. Townsend, S. J. Field, D. C. Hanna, D. P. Shepherd, and A. C. Tropper, J. Appl. Phys. **69**, 3440 (1991).
[18]V. Mussi, F. Somma, P. Moretti, J. Mugnier, B. Jacquier, R. M. Montereali, and E. Nichelatti, Appl. Phys. Lett. **82**, 3886 (2003).
[19]J. Rams, J. Olivares, P. J. Chandler, and P. D. Townsend, J. Appl. Phys. **87**, 3199 (2000).
[20]S. Kostritskii and P. Moretti, J. Appl. Phys. **101**, 094109 (2007).
[21]G. Fu, K.-M. Wang, F. Cheng, X.-L. Wang, S.-L. Li, D.-Y. Shen, H.-J. Ma, and R. Nie, Nucl. Instrum. Methods Phys. Res. B **211**, 346 (2003).
[22]F.-X. Wang, F. Chen, X.-L. Wang, Q.-M. Lu, K.-M. Wang, D.-Y. Shen, H.-J. Ma, and R. Nie, Nucl. Instrum. Methods Phys. Res. B **215**, 389 (2004).
[23]G. V. Vázquez, J. Rickards, G. Lifante, M. Domenech, and E. Cantelar, Opt. Express **11**, 1291 (2003).
[24]F. Chen, H. Hu, J.-H. Zhang, F. Lu, B.-R. Shi, K.-M. Wang, D.-Y. Shen, and Ch.-Q. Wang, Phys. Status Solidi A **187**, 543 (2001).
[25]D. Fluck, P. G¸nter, R. Irmscher, and Ch. Buchal, Appl. Phys. Lett. **59**, 3213 (1991).
[26]M. L. von Bibra, A. Roberts, and S. D. Dods, Nucl. Instrum. Methods Phys. Res. B **168**, 47 (2000).
[27]See http://www.srim.org/ for the calculation programs.
[28]A. Boudrioua and J. C. Loulergue, Opt. Commun. **137**, 37 (1997).
[29]J. B. Gruber, M. E. Hills, R. M. Macfarlane, C. A. Morrison, G. A. Turner, G. J. Quarles, G. J. Kintz, and L. Esterowitz, Phys. Rev. B **40**, 9464 (1989).
[30]J. A. Koningstein and J. E. Geusic, Phys. Rev. **136**, A711 (1964).
[31]N. Rakov, G. S. Maciel, M. L. Sundheimer, L de S. Menezes, A. S. L. Gomes, Y. Messaddeq, F. C. Cassanjes, G. Poirier, and S. J. L. Ribetro, J. Appl. Phys. **92**, 6337 (2002).